Supplementary Information

Aptamer-based Colorimetric, and Lateral Flow Assay Approaches for the Detection of Toxic Metal Ions, Thallium(l) and Lead(ll).

Sathya Srinivasan[a,b], Velu Ranganathan[a], Erin M. McConnell[a], Bhaskar Mohan Murari[c,*], Maria C. DeRosa[a,*]

a Department of Chemistry, Carleton University, 1125 Colonel By Drive, Ottawa, ON K1S 5B6, Canada
b Department of Biotechnology, School of Bioscience and Technology, VIT, Vellore, 632 104, TN, India
c Department of Sensor and Biomedical Technology, School of Electronics Engineering, VIT, Vellore, 632 104, TN, India

*Correspondence: maria.derosa@carleton.ca (M.C.D.); Tel: +1-613-520-2600 (ext. 3844) (M.C.D.).

1.1 Sequences of aptamers [1–3] used in this work

Table S1 The aptamer Sequences used in this work

Name	**Sequences from 5' to 3'**
Thallium aptamer [1]	5' - GTG GGT AGG GCG GGT TGG - 3'
Biotin modified Thallium aptamer	5' - Biotin-GTG GGT AGG GCG GGT TGG - 3'
Lead aptamer[2,3]	5' - GGG TGG GTG GGT GGG T – 3'
Biotin modified Lead aptamer	5' - Biotin- GGG TGG GTG GGT GGG T – 3'

1.2 Gold nanoparticles (AuNPs) synthesis

Procedures for colloidal gold nanoparticle preparation were the same as those developed by Grabar et. al., [4] with modification to the volume of $HAuCl_4$ and sodium citrate, since higher $HAuCl_4$ concentration leads to larger colloids [5]. All glassware used for AuNP synthesis was cleaned by soaking in aqua regia (3:1 mixture of concentrated HCl/HNO_3) for 15 minutes followed by thorough rinsing with deionized water. A 250 mL Erlenmeyer flask was used to mix 98 mL of deionized water and 2 mL of 50 mM $HAuCl_4$ to a final concentration of 1 mM $HAuCl_4$. The

solution was heated to boiling with stirring. Once boiling, 10 mL of 38.8 mM sodium citrate was added. Following the change in suspension colour from pale yellow to dark blue and finally to a wine red, heating was continued for an additional 20 minutes. The flask was removed from the heat and allowed to cool to room temperature with continued stirring. The nanoparticles were quantified by UV-Vis.

1.3 Silver nanoparticle (AgNPs) synthesis

The AgNPs were synthesized by a citrate-capped AgNPs method following a procedure reported in the literature [6,7]. Briefly, $AgNO_3$ (250 µL of 100 mM) and trisodium citrate (250 µL of 100 mM) were added into 100 mL of water under stirring. 6 mL of freshly prepared 5 mM $NaBH_4$ was added into the above aqueous solution under vigorous stirring. The resulting yellow colloidal AgNPs solution was further stirred for 30 minutes and solution was cooled to room temperature. Finally, the AgNPs were purified by centrifugation at 14000 rpm for 30 minutes to remove the excess citrate molecules in the supernatant solution. The AgNPs had plasmon absorption peaks around 400 nm.

1.4 HR-TEM Analysis

The adsorption-desorption mechanism for the AuNP-aptamer complex was fully supported by HR-TEM and histogram analysis. The TEM samples of AuNP-aptamer complex in the absence and presence of Tl(I) were prepared by drop-casting a dilute suspension on a carbon-coated copper grid. In the absence of Tl(I), the AuNP-aptamer complexes were well-dispersed and aggregates were not observed (Fig. S6a) and corresponding histogram (Fig. S6b). Upon the addition of Tl(I) (150 µM), the nanoparticles aggregates were observed (Fig. S6c) and corresponding histogram (Fig. S6d) due to the specific binding of Tl(I) to the aptamer. Similar observations were noted of AuNP-aptamer in the absence and presence of Pb(II) (Fig. S7). TEM images indicated that the aptamer-AgNPs are well dispersed with a diameter of 12 nm. The TEM measurements for the AgNP-aptamer complex in the absence and presence of Tl(I) and Pb(II) were carried out using the same concentrations and conditions listed above to perform AuNP-aptamer complex. Similar observations were noted of AgNP-aptamer complex (Fig. S8 and Fig. S9).

Figures

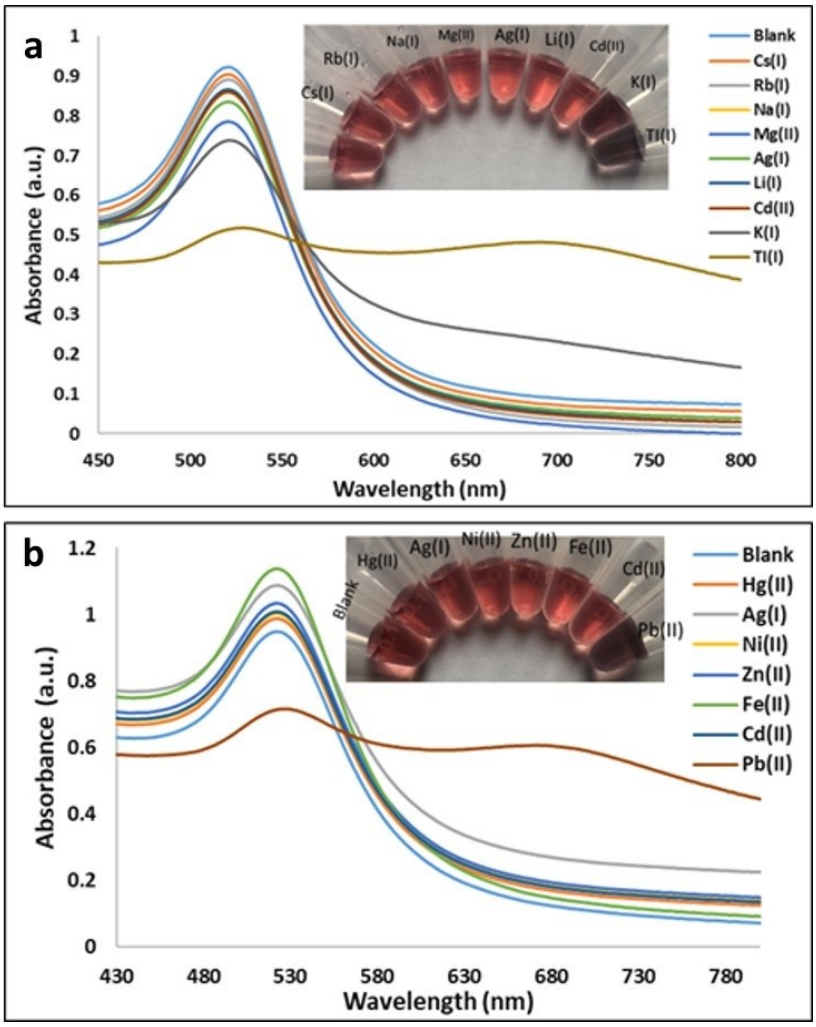

Fig. S1 a). The absorption spectra of Tl(I)-aptamer/AuNP complexes with various metal ions, (inset) the corresponding visual color solutions. All the metal ions concentrations were 120 µM. b). The absorption spectra of Pb(II)-aptamer/AuNP complexes with various metal ions, (inset) the corresponding visual color solutions. All the ion concentrations were 150 nM. Triplicate experiments were performed.

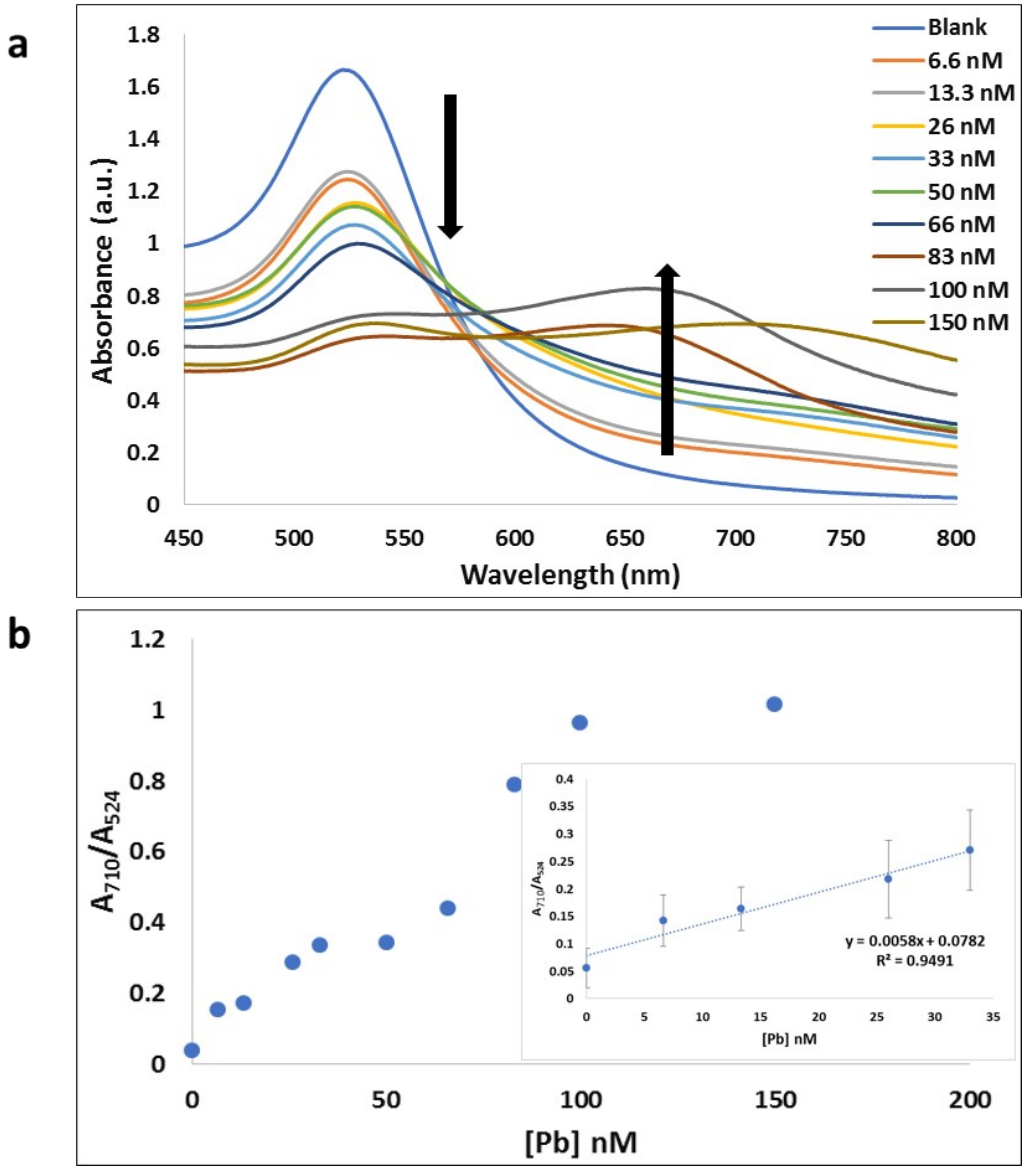

Fig. S2 a). Pb(II)-aptamer/AuNP complex absorption spectra under increasing concentrations of Pb(II) ions (0-150 nM).The calibration curve displays the ratio of absorbance at 710 nm to 524 nm versus respective Pb(II) ion concentrations. The inset illustrates the linear dynamic range.

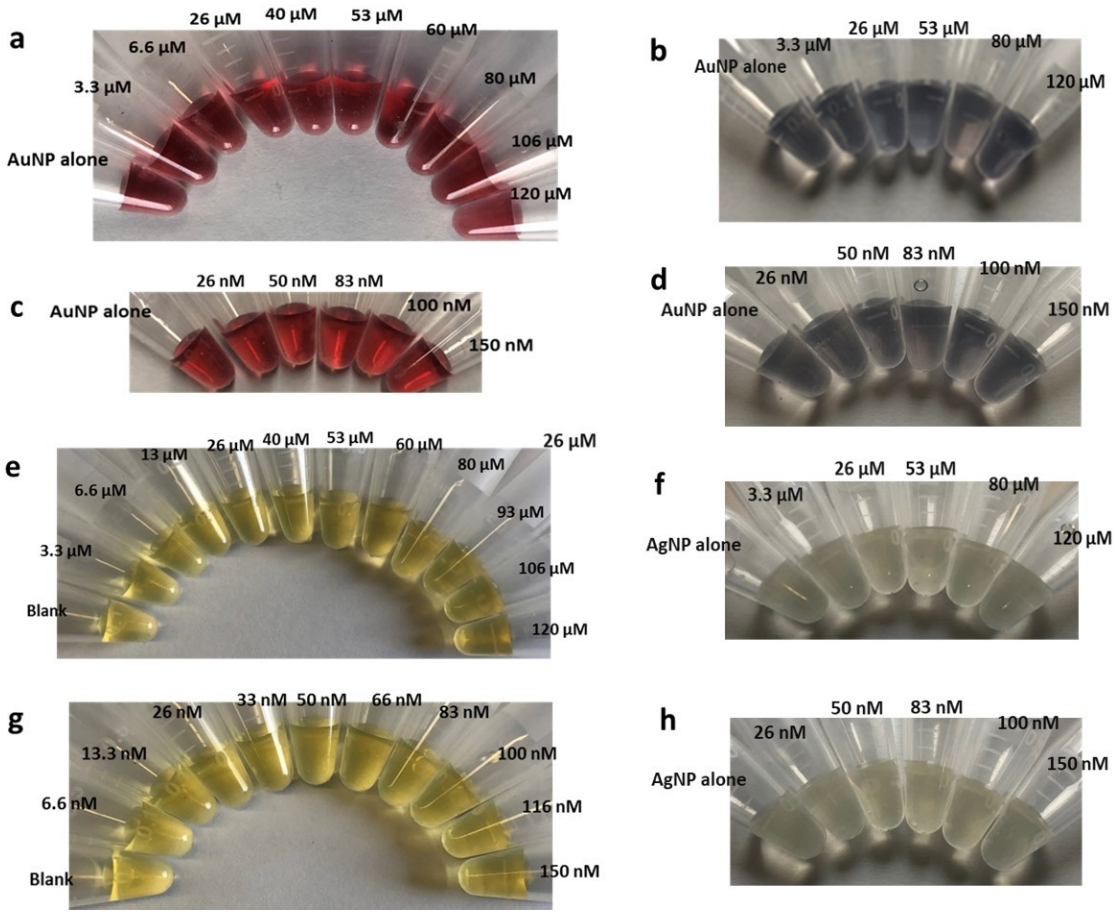

Fig. S3. The effect of increasing concentrations of metal ions with metal nanoparticles in the absence and presence of NaCl: AuNPs in the presence of various concentrations (0-120 µM) of Tl(I) in the absence and presence of salt (a & b). AuNPs in the presence of various concentrations (0-150 nM) of Pb(II) in the absence and presence of salt (c&d). AgNPs in the presence of various concentrations (0-120 µM) of Tl(I) in the absence and presence of salt (e & f). AgNPs in the presence of various concentrations (0-150 nM) of Pb(II) in the absence and presence of salt (g & h).

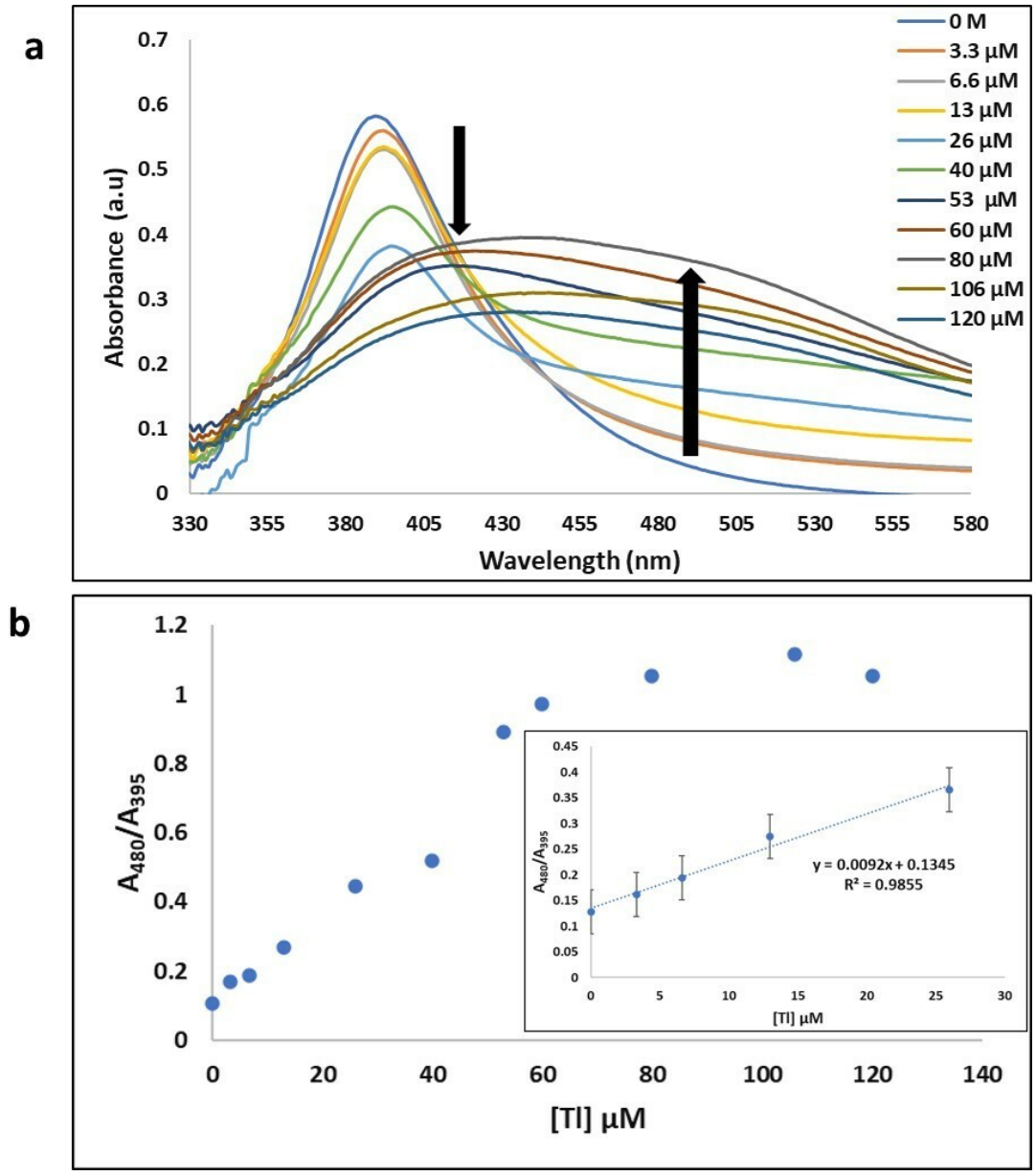

Fig. S4 a). TI(I)-aptamer/AgNP complex absorption spectra under increasing concentrations of Tl(I) ions (0-120 µM). b). The calibration curve displays the ratio of absorbance at 480 nm to 395 nm versus respective Tl(I) ion concentrations. The inset illustrates the linear dynamic range.

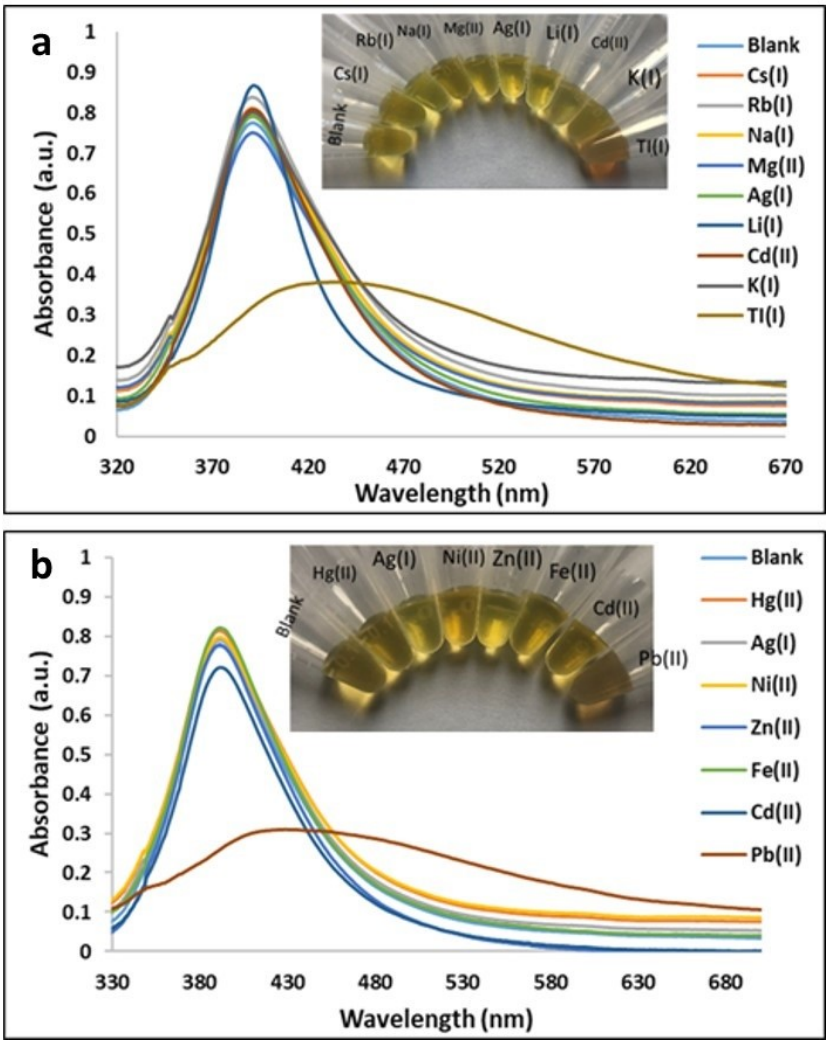

Fig. S5 a). The absorption spectra of Tl(I)-aptamer-AgNP complexes with various metal ions, (inset) the corresponding visual color solutions. All the metal ions concentrations were 120 µM. b). The absorption spectra of Pb(II)-aptamer-AgNP complexes with various metal ions, (inset) the corresponding visual color solutions. All the ion concentrations were 150 nM. Triplicate experiments were performed.

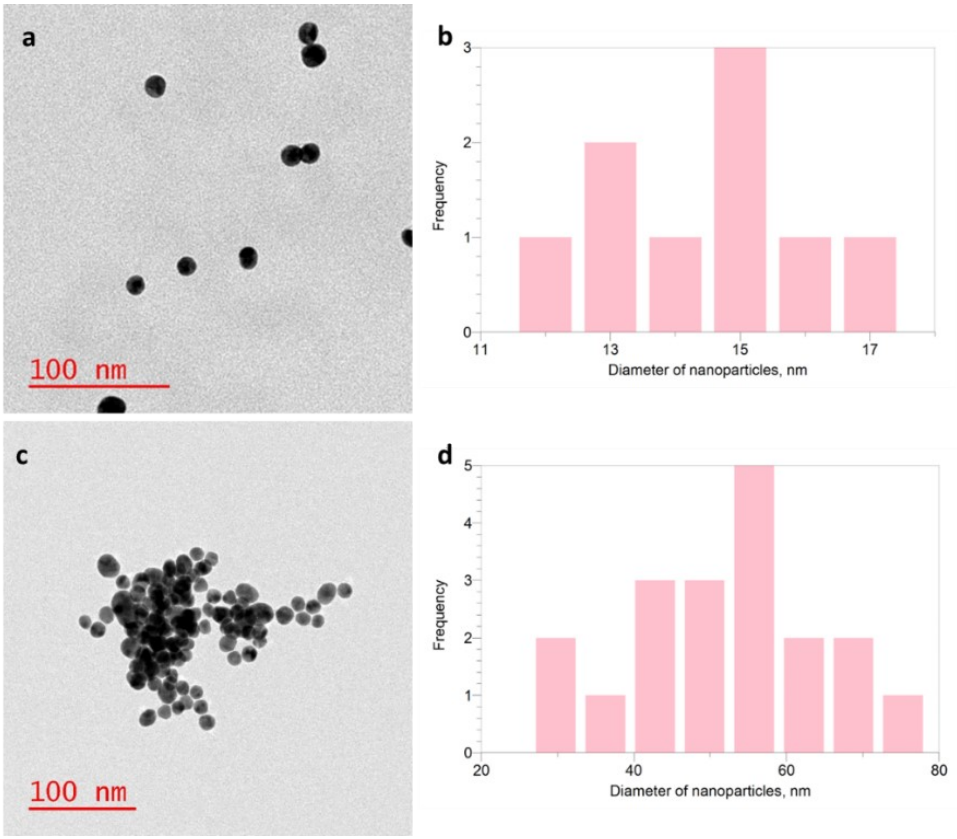

Fig. S6 TEM images and histograms: HR-TEM images of the Tl(I)-binding aptamer and AuNPs (aptamer-AuNPs) well dispersed of the AuNPs (a). After the addition of Tl(I), the images showing the aggregated AuNPs (c). Corresponding histograms of AuNP-aptamer and AuNP-aptamer/Tl(I) (band d). Conditions: 0.4 μM aptamer, AuNPs (3.86 nM), Tl(I) (150 μM) and NaCl (50 mM).

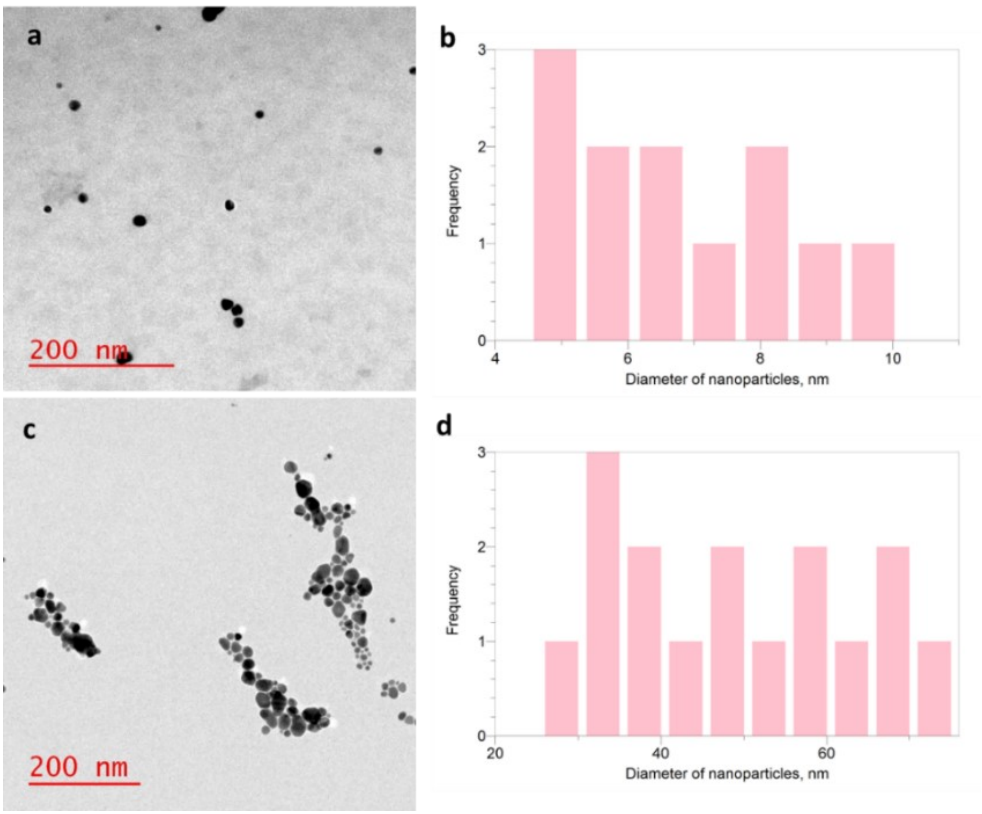

Fig. S7 TEM images and histograms: HR-TEM images of the Tl(I)-binding aptamer and AgNPs (aptamer-AgNPs) well dispersed of the AgNPs (a). After the addition of Tl(I), the images showing the aggregated AgNPs (c). Corresponding histograms of AgNP-aptamer and AgNP-aptamer/Tl(I) (band d). Conditions: 0.4 μM aptamer, AgNPs (3 nM), Tl(I) (150 μM) and NaCl (60 mM).

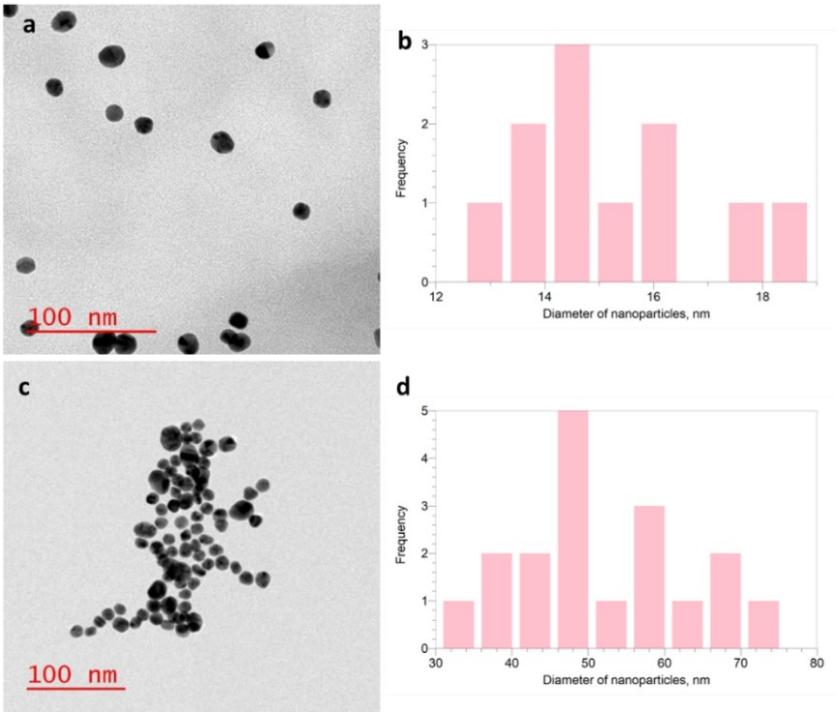

Fig. S8 TEM images and histograms: HR-TEM images of the Pb(II)-binding aptamer and AuNPs (aptamer-AuNPs) well dispersed of the AuNPs (a). After the addition of Pb(II), the images showing the aggregated AuNPs (c). Corresponding histograms of AuNP-aptamer and AuNP-aptamer/Pb(II) (b and d). Conditions: 0.4 μM aptamer, AuNPs (3.86 nM), Pb(II) (150 nM) and NaCl (50 mM).

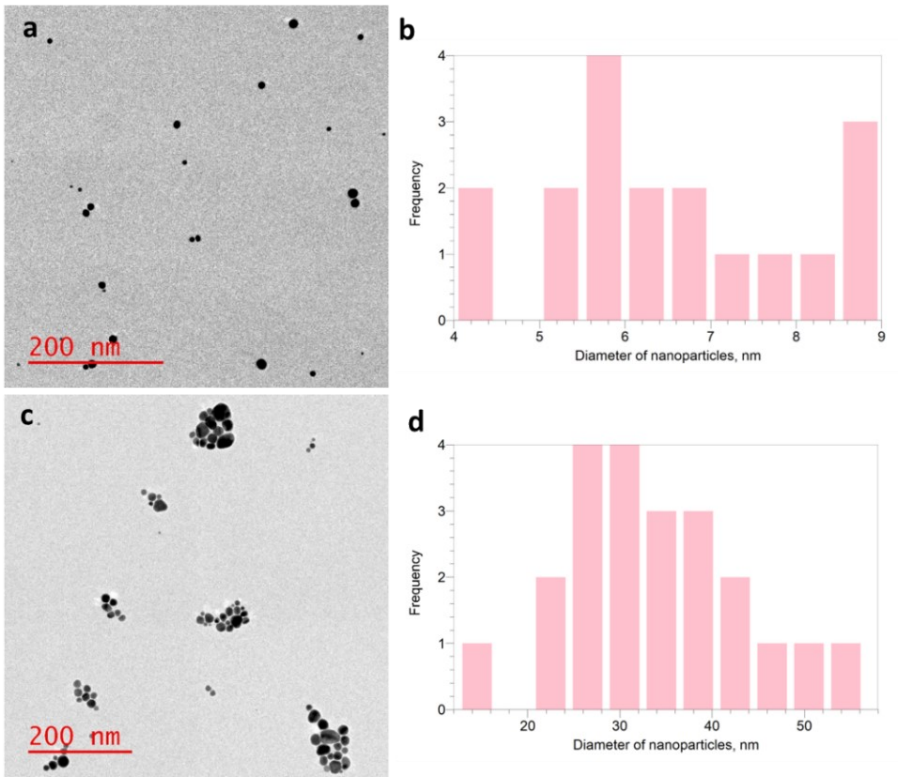

Fig. S9 TEM images and histograms: HR-TEM images of the Pb(II)-binding aptamer and AgNPs (aptamer-AgNPs) well dispersed of the AgNPs (a). After the addition of Pb(II), the images showing the aggregated AgNPs (c). Corresponding histograms of AgNP-aptamer and AgNP-aptamer/Pb(II) (b and d). Conditions: 0.4 μM aptamer, AgNPs (3 nM), Pb(II) (150 nM) and NaCl (60 mM).

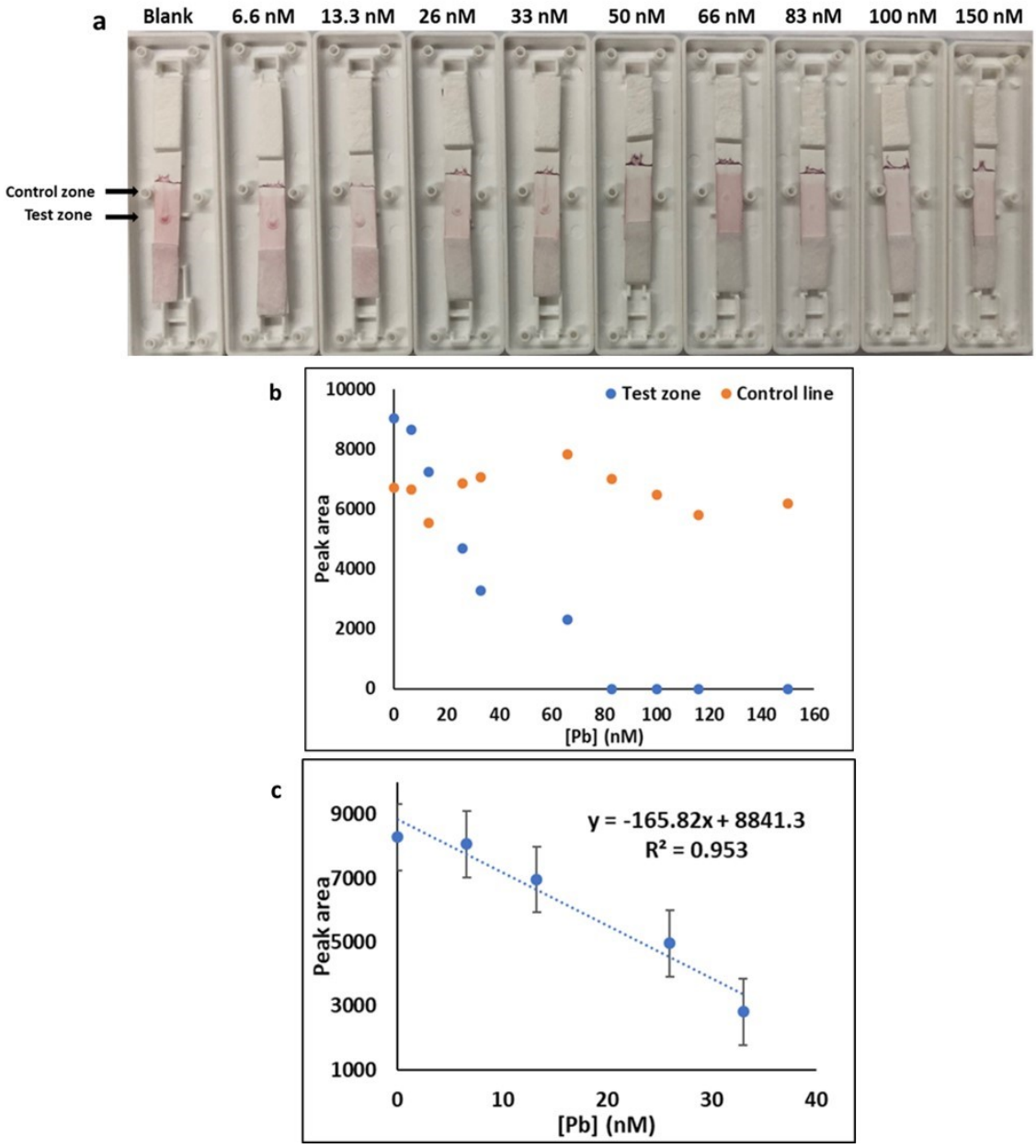

Fig. S10 a). The LFA (AuNPs based) for the detection of Pb(II) with various concentrations of Pb(II) (ranges from 0-150 nM). b). The calibration curve was plotted against to the peak area (test (T) and control (C) zones vs various Pb(II) concentrations were analyzed by ImageJ software. c) The linear dynamic range.

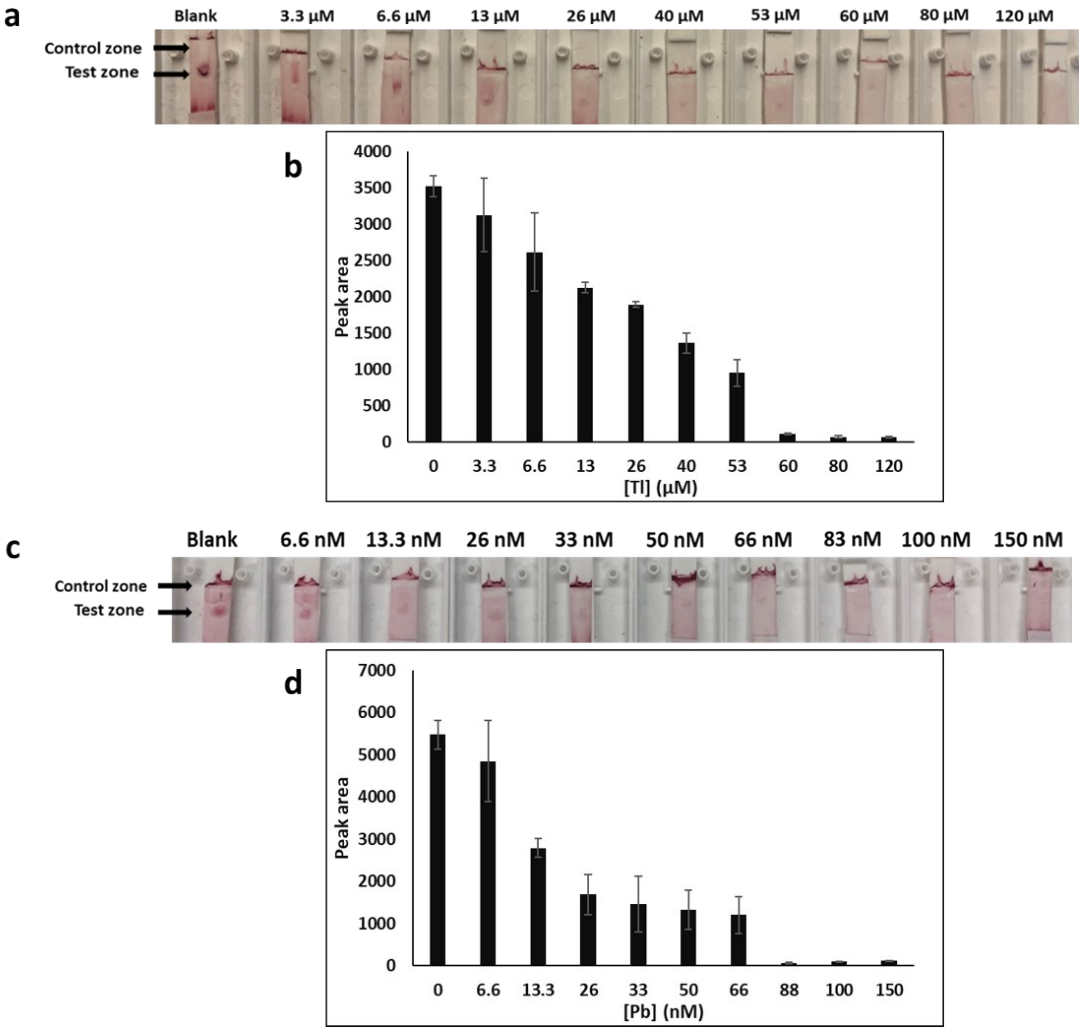

Fig. S11 a). The LFA (AuNPs based) for the detection of river water spiked with Tl(I) with various concentrations of Tl(I) (from 0- 120 µM). b). The histogram of corresponding peak area test (T) zone vs different Tl(I) concentrations were analyzed by ImageJ software. c). The photograph of the LFA (AuNPs based) for river water spiked with Pb(II) with different concentrations of Pb(II) (from 0- 150 nM). d). The histogram of corresponding peak area test zone(T) vs different Pb(II) concentrations.

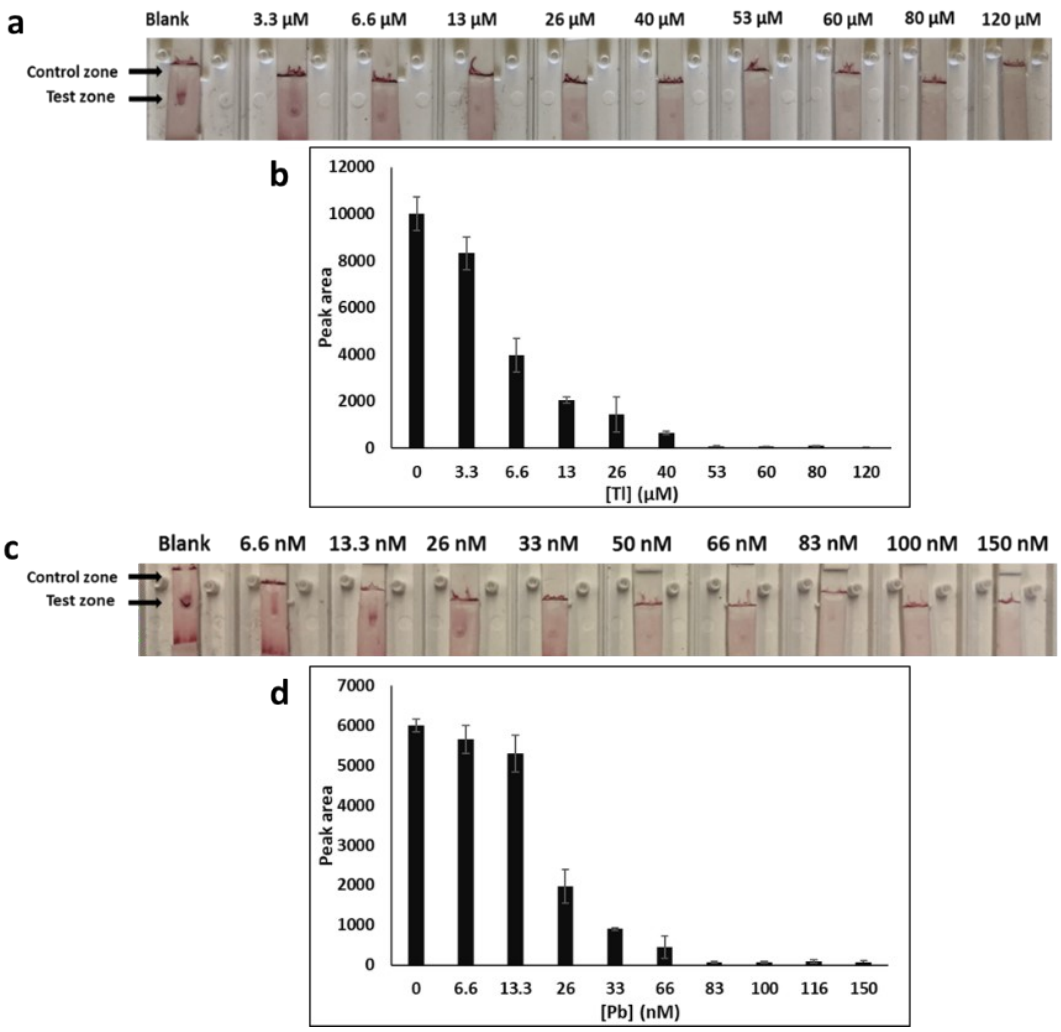

Fig. S12 a). The LFA (AuNPs based) for the detection of serum sample spiked with Tl(I) with various concentrations of Tl(I) (from 0- 120 µM). b). The histogram of corresponding peak area of the test zone (T) vs various Tl(I) concentrations were analyzed by ImageJ software. c). The photograph of the LFA (AuNPs based) for serum sample spiked with Pb(II) with various concentrations of Pb(II) (from 0- 150 nM). d). The histogram of corresponding peak area of the test zone (T) vs different Pb(II) concentrations.

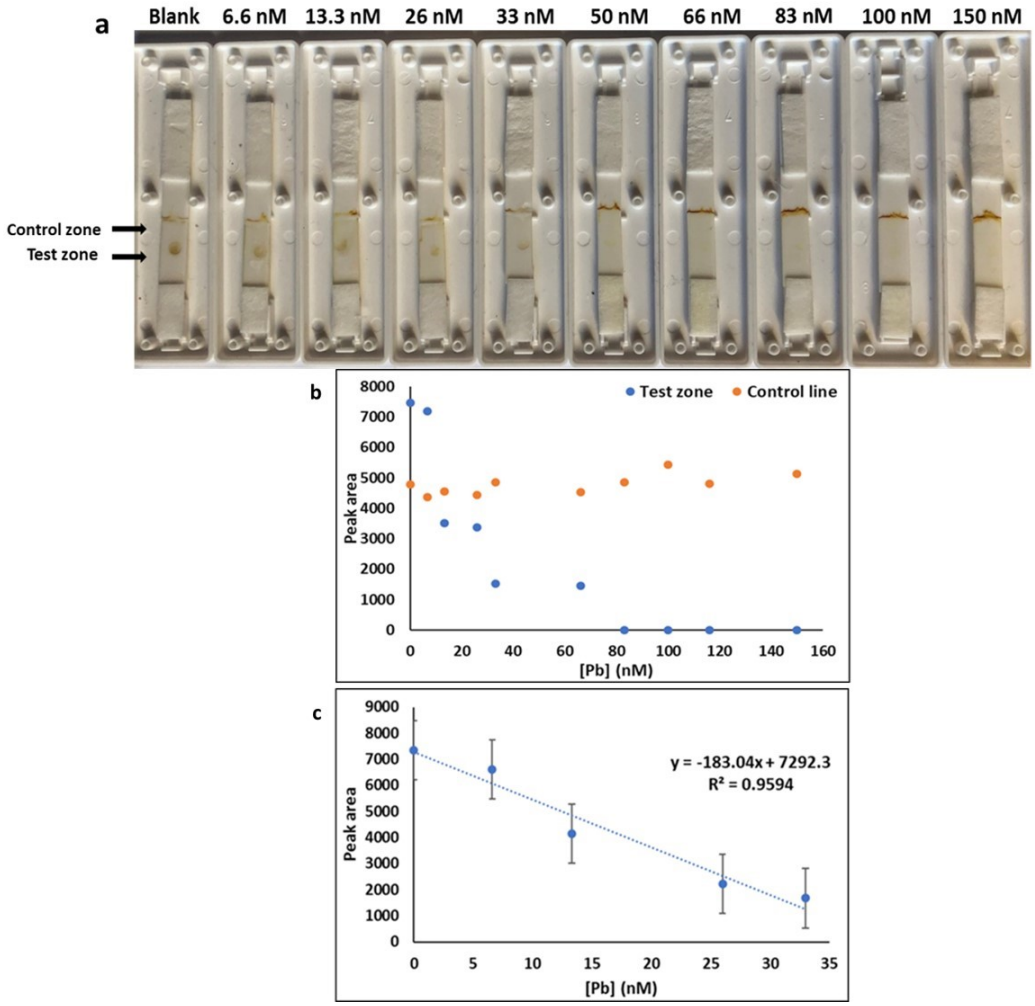

Fig. S13 a). The LFA (AgNPs based) for Pb(II) with various concentrations of Pb(II) (ranges from 0-150 nM). b). The calibration curve was plotted corresponding to the peak area of the test (T) zone vs various Pb(II) concentrations were analyzed by ImageJ software. c) shows linear dynamic range.

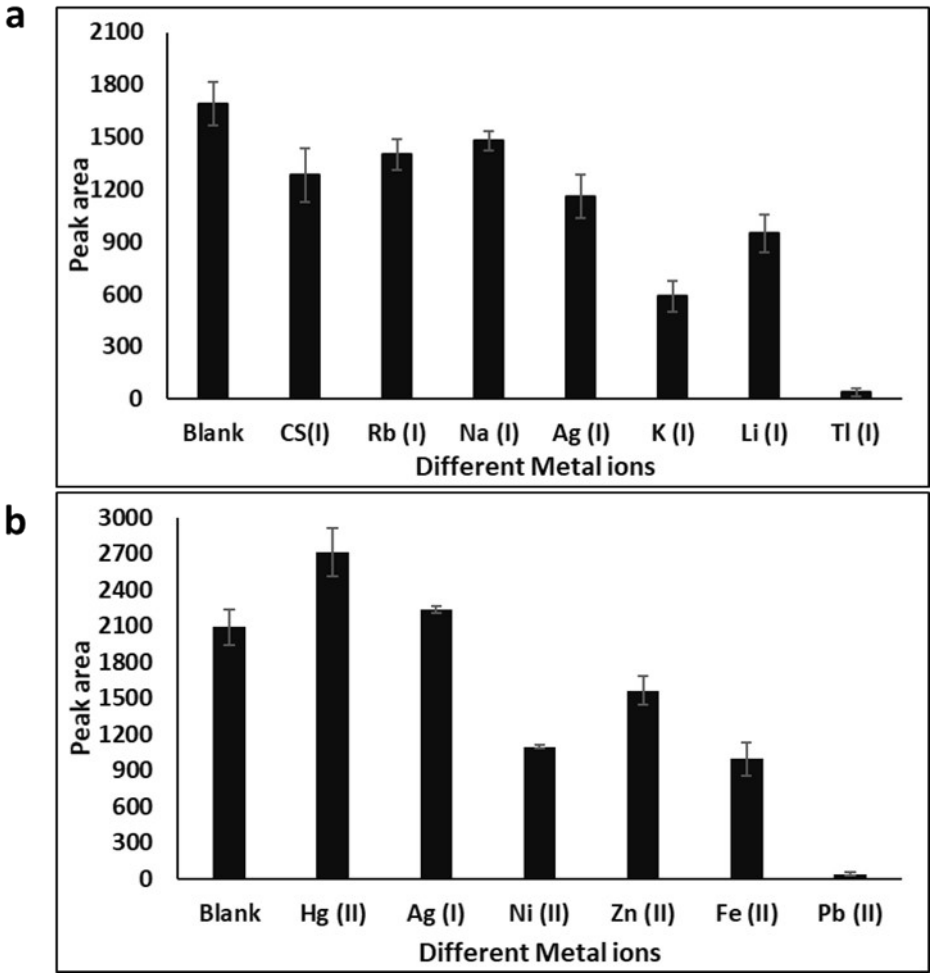

Fig. S14 a.) The AgNPs based LFA selectivity experiments for Tl(I) over Rb(I), Cs(I), Na(I), K(I), Ag(I) and Li(I). All the metal ions concentrations were 120 µM. b). The AgNPs based LFA selectivity experiments for Pb(II) over Zn(II), Hg(II), Ni(II), Ag(I) and Fe(II). All the ion concentrations were 150 nM. Triplicate experiments were performed. The histogram of corresponding peak area test (T) zone vs various metal ions were analyzed by ImageJ software.

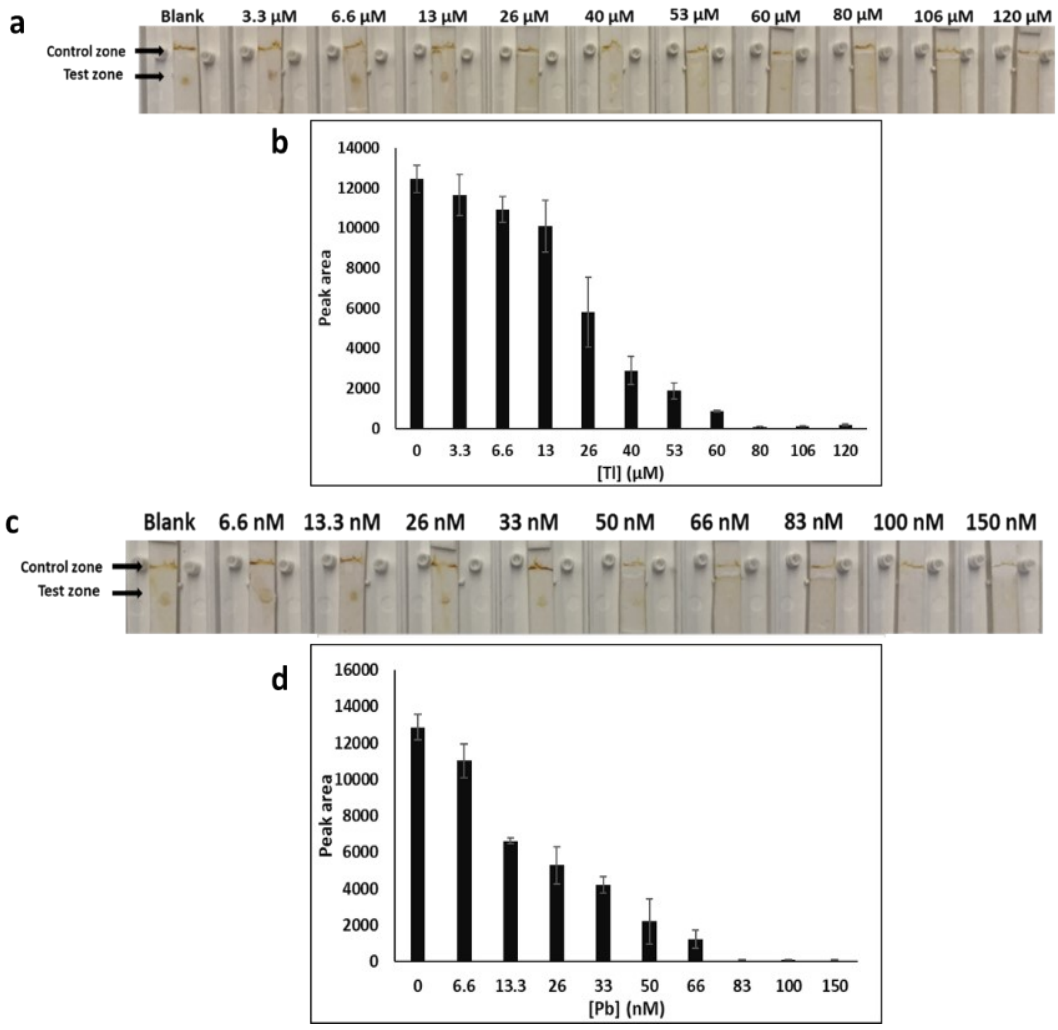

Fig. S15 a). The LFA (AgNPs based) for river water spiked with Tl(I) with various concentrations of Tl(I) (from 0- 120 µM). b). The histogram of corresponding peak area test (T) zone vs different Tl(I) concentrations were analyzed by ImageJ software. c). The photograph of the LFA (AgNPs based) for river water spiked with Pb(II) with various concentrations of Pb(II) (from 0- 150 nM). d). The histogram of corresponding peak area test (T) zone vs different Pb (II) concentrations.

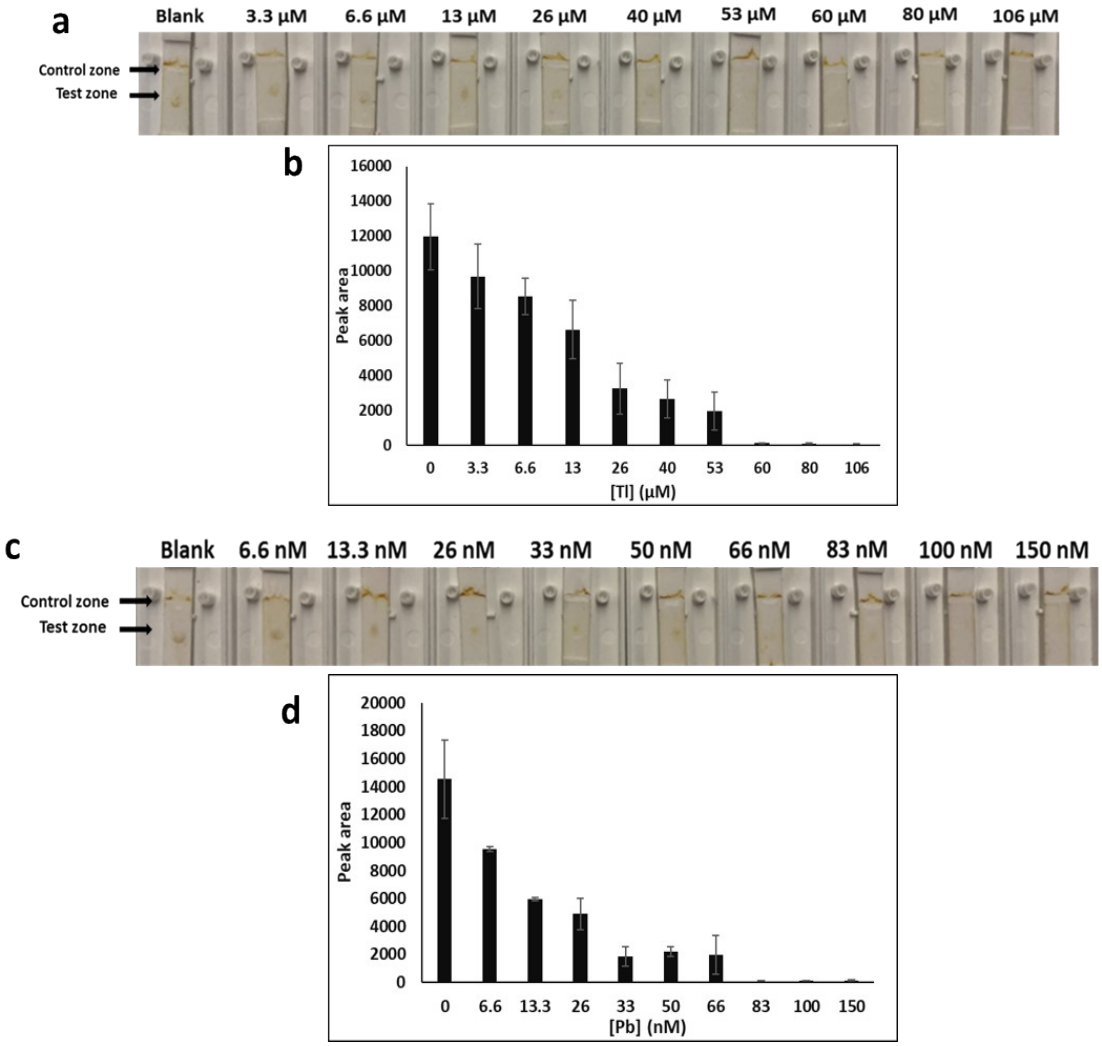

Fig. S16 a). The LFA (AgNPs based) for the detection of serum sample spiked with Tl(I) with various concentrations of Tl(I) (from 0- 120 µM). b). The histogram of corresponding peak area of the (test (T)) zone vs various Tl(I) concentrations were analyzed by ImageJ software. c). The photograph of the LFA (AgNPs based) for the detection of serum sample spiked with Pb(II) with various concentrations of Pb(II) (range from 0- 150 nM). d). The histogram of corresponding peak area of the (test (T)) zone vs various Pb(II) concentrations.

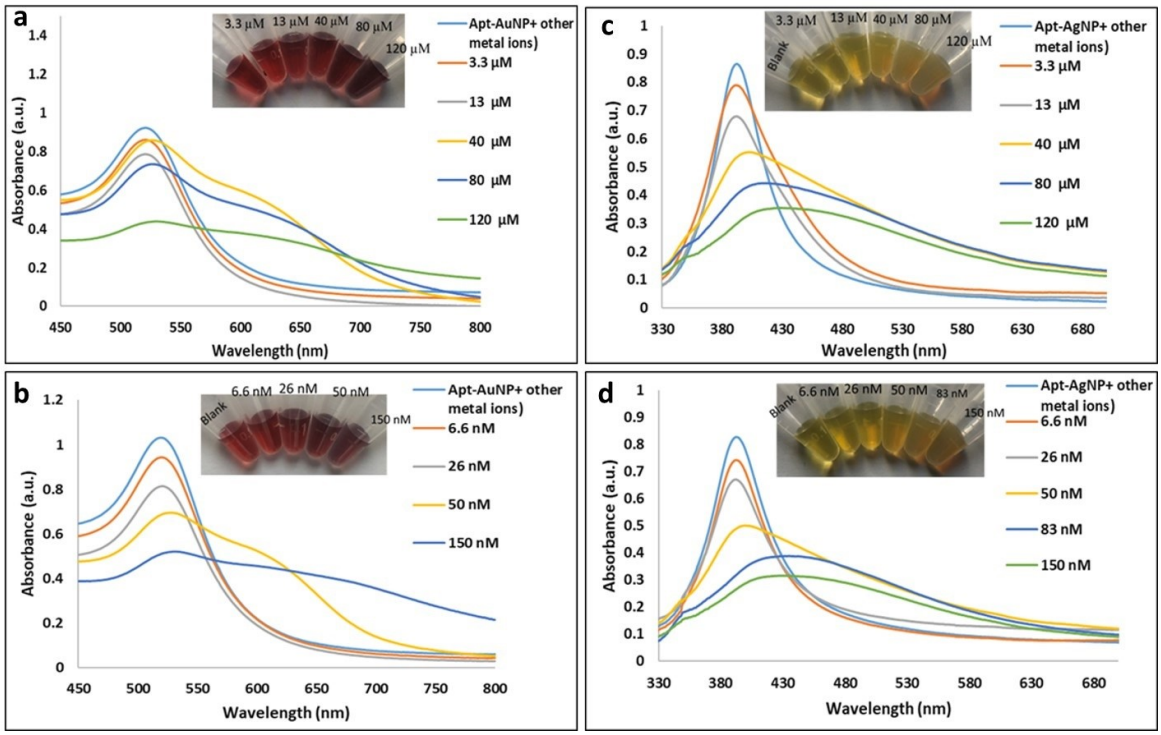

Fig. S17 Competitive titration. a and b). TI(I)-aptamer/AuNP complex and Pb(II)-aptamer/AuNP complex absorption spectra under increasing concentrations of Tl (I) (0-120 µM) and Pb(II) ions (0-150 nM) in the presence of 5-fold excess of other metal ions. c and d). TI(I)-aptamer/AgNP complex and Pb(II)-aptamer/AgNP complex absorption spectra under increasing concentrations of Tl (I) (0-120 µM) and Pb(II) ions (0-150 nM) in the presence of 5-fold excess of other metal ions.

References

1 M. Hoang, P. J. J. Huang and J. Liu, *ACS Sensors*, 2016, **1**, 137–143.

2 S. M. Taghdisi, N. M. Danesh, P. Lavaee, A. S. Emrani, M. Ramezani and K. Abnous, *RSC Adv.*, 2015, **5**, 43508–43514.

3 S. M. Taghdisi, S. S. Emrani, K. Tabrizian, M. Ramezani, K. Abnous and A. S. Emrani, *Environ. Toxicol. Pharmacol.*, 2014, **37**, 1236–1242.

4 K. C. Grabar, M. B. Hommer, M. J. Natan and R. G. Freeman, *Anal. Chem.*, 1995, **67**, 735–743.

5 J. Chamberlain, M. N. Afsar and J. B. Hasted, *Nature*, 1973, **244**, 47–49.

6 R. C. Doty, T. R. Tshikhudo, M. Brust and D. G. Fernig, *Chem. Mater.*, 2005, **17**, 4630–4635.

7 D. Paramelle, A. Sadovoy, S. Gorelik, P. Free, J. Hobley and D. G. Fernig, *Analyst*, 2014,

139, 4855–4861.